J. Fluid Mech. (1993), *vol.* 247, *pp.* 205–229

Trapped internal gravity waves in a geostrophic boundary current

By HONG MA†

Department of Atmospheric, Oceanic and Space Sciences and Laboratory for Scientific Computing, The University of Michigan, Ann Arbor, MI 48109, USA

(Received 2 December 1991 and in revised form 27 July 1992)

The effect of a geostrophic boundary current on internal gravity waves is studied with a reduced-gravity model. We found that the boundary current not only modifies the coastal Kelvin wave, but also forms wave guides for short internal gravity waves. The combined effects of current shear, the boundary, and the slope of the interface create the trapping mechanism. These trapped internal gravity waves appear as groups of discrete zonal modes. They have wavelengths comparable to or shorter than the internal Rossby radius of deformation. Their phase speeds are close to that of the internal Kelvin wave. However, they can propagate both in, or opposite to, the direction of the Kelvin wave. The results of the present work suggest the possibility of finding an energetic internal gravity wave phenomenon with near-inertial frequency in a broad geostrophic boundary current.

1. Introduction

Theoretical studies of water wave and current interaction started half a century ago when Unna (1942) studied the effect of tidal streams on waves, although observations of this physical phenomenon might have been made for centuries. Johnson (1947) also discussed the refraction mechanism caused by wave–current interaction, and suggested that the major ocean currents might have an important impact on the characteristics of waves, i.e. wave height, wavelength, and the directions in which they approach the shore. Longuet-Higgins & Stewart (1960, 1961) found that a short wave underwent changes in its amplitude and wavelength when it interacted with non-uniform currents or long waves. Kenyon (1971) used the geometrical optics approximation to study the refraction of surface gravity waves in ocean currents, and applied his theory to analysing the trapping and reflection of gravity waves in the Gulf Stream and the Circumpolar Current. Peregrine & Smith (1975) developed asymptotic solutions for stationary gravity waves in jet-like streams. Their treatment of trapped surface waves was an extension of the work of Smith (1970). In their problem, the waves were 'doubly' trapped at both the surface and the centre of the jet. Kunze (1985) used the ray tracing approach to show the behaviour of near-inertial waves in a model geostrophic jet. He found that trapping occurred in regions of negative vorticity. Comprehensive reviews of gravity waves and current interaction are given by Peregrine (1976), and more recently by Jonsson (1989).

So far, most studies on water wave and current interaction problems can be applied only to the interior of the ocean (lake) because they do not consider the effect

† Present address: Department of Applied Science, Building 515, Brookhaven National Laboratory, Upton, NY 11973, USA.

of the horizontal boundaries of the basin. The lack of study on wave interaction with coastal currents is partly due to the mathematical difficulties involved, e.g. considering continuous stratification and horizontal-boundary conditions at the same time usually results in non-separable equations, and is also probably partly due to the fact that the relative importance of mean currents in coastal region is not fully understood. Grimshaw (1983) studied the effect of a depth-dependent mean current, which has no horizontal shear, on Kelvin waves in a stratified ocean. He found that the Kelvin wave in a vertically sheared mean current contained all vertical modes. Later, Grimshaw & Yi (1990) studied the coastal current effect on long waves, and their results provided fully nonlinear wave-like solutions. They pointed out, however, that the long-wave restriction of their results precluded their theory from being applicable directly to observations because the alongshore scale and offshore scale were comparable in observed meanders.

In the present work, we used a $1\frac{1}{2}$ layer reduced-gravity model to study trapped internal gravity waves in a geostrophically balanced, steady boundary current, which exists only in the upper layer and flows parallel with the straight coastline (Ma 1991).

At low frequencies (compared with the inertial frequency), the only kind of trapped waves allowed by the present model are the internal Kelvin waves. In §3, we derive estimates of the effect of the current on the speed and offshore shape of the internal Kelvin wave of a given longshore wavenumber.

At high frequencies, trapped internal gravity waves propagating alongshore are possible, as members of a group of discrete offshore modes (the mode number equals the number of zero-crossings in the offshore direction). In some cases, high-frequency internal gravity waves can be trapped in a mid-ocean wave guide, which is formed by two interior turning points in the offshore direction. The location of the wave guide depends on the structures of the mean current and the associated interface slope. In §4, asymptotic formulae for the wave dispersion relationship, modal shapes, and locations of the wave guide are derived for the high-frequency end of the spectrum.

Although asymptotic formulae are obtained for both the low and high ends of the spectrum, we also solved the problem numerically. Numerical solutions here serve not only as substitutes when asymptotic solutions are difficult to obtain or the asymptotic condition is not met, but also as tests of the correctness of the asymptotic methods. The numerical technique used in this paper is the Chebyshev spectral method, which was extended by Boyd (1989) to solve infinite and semi-infinite domain problems.

2. Model assumptions and non-dimensionalization

The present model has the following features:

(i) a half-planar ocean (infinite in the meridional direction, and semi-infinite in the zonal direction) in the northern hemisphere, on which a coordinate system is set in such a way that its x- and y-axes point to the east and north respectively. The eastern boundary is located at $x = 0$ (the choice of the north–south orientation of the coastal line is for convenience, which does not affect the generality of the present study);

(ii) two layers of homogeneous fluid, the top layer is of depth H which is always positive (no outcropping), and the deep lower layer is motionless and has a slightly higher density;

(iii) the fluid is inviscid and incompressible;

(iv) the hydrostatic approximation and f-plane assumption are adopted;

(v) in the steady state, there is a geostrophic meridional current which is confined within the top layer and has only zonal shear.

Under these assumptions, the shallow-water equations become

$$\frac{\partial u}{\partial t}+u\frac{\partial u}{\partial x}+(v+\bar{v})\frac{\partial u}{\partial y}-fv=-g'\frac{\partial \eta}{\partial x}, \tag{2.1}$$

$$\frac{\partial v}{\partial t}+u\frac{\partial (v+\bar{v})}{\partial x}+(v+\bar{v})\frac{\partial v}{\partial y}+fu=-g'\frac{\partial \eta}{\partial y}, \tag{2.2}$$

$$\frac{\partial \eta}{\partial t}+\frac{\partial}{\partial x}\{u[\eta+\bar{h}+H_0]\}+\frac{\partial}{\partial y}\{(v+\bar{v})[\eta+\bar{h}+H_0]\}=0, \tag{2.3}$$

where g' is the reduced gravity; f is the Coriolis parameter; u and v are the offshore and alongshore velocities in the top layer, respectively, which are caused by the wave motion; $\bar{v}(x)$ is the mean current velocity, which is in geostrophic balance, i.e. $f\bar{v}(x)=g'\,\mathrm{d}\bar{h}(x)/\mathrm{d}x$; $\bar{h}(x)$ is the variation of the interface depth due to the geostrophic mean current; $\bar{h}(x)+H_0=H(x)$ is the mean thickness of the layer, and H_0 is its value at the eastern boundary, which is chosen for convenience; and $\eta(x,y,t)$ is the interface displacement from the mean.

Now we define the non-dimensionalized variables as

$$(\bar{v},u,v)=(g'H_0)^{\frac{1}{2}}(u^*,v^*,v^*)=C(\bar{v}^*,u^*,v^*),$$
$$(\bar{h},\eta)=H_0(\bar{h}^*,\eta^*),$$
$$(x,y)=[(g'H_0)^{\frac{1}{2}}/f](x^*,y^*)=L_{\mathrm{R}}(x^*,y^*),$$
$$t=t^*/f=Tt^*.$$

Therefore, the non-dimensionalization scales C, L_{R} and $1/T$ are the internal Kelvin wave speed, the internal Rossby radius of deformation, and the inertial frequency, respectively. If we take $f=3\times10^{-4}\ \mathrm{s}^{-1}$, $(\rho_2-\rho_1)/\rho_2=0.005$ (where ρ_1 and ρ_2 are the densities of the top layer and the lower layer, respectively) and $H_0=50$ m, then $C=2.7\ \mathrm{m\ s^{-1}}$ and $L_{\mathrm{R}}=27$ km.

Substituting the above expressions into (2.1)–(2.3) and omitting the asterisks for simplicity, we obtain the non-dimensionalized shallow-water equations

$$\frac{\partial u}{\partial t}+u\frac{\partial u}{\partial x}+(v+\bar{v})\frac{\partial u}{\partial y}-v=-\frac{\partial \eta}{\partial x}, \tag{2.4}$$

$$\frac{\partial v}{\partial t}+u\frac{\partial (v+\bar{v})}{\partial x}+(v+\bar{v})\frac{\partial v}{\partial y}+u=-\frac{\partial \eta}{\partial y}, \tag{2.5}$$

$$\frac{\partial \eta}{\partial t}+\frac{\partial}{\partial x}[u(\eta+\bar{h}+1)]+\frac{\partial}{\partial y}[(v+\bar{v})(\eta+\bar{h}+1)]=0. \tag{2.6}$$

3. Mean current effect on the coastal Kelvin wave

3.1. *Perturbation equations*

We used the perturbation method to study the shear mean current effect on the coastal Kelvin wave. If we assume that the wave field is of sinusoidal wave form in

the y (meridional) direction, then the wave and the mean current can be expressed as

$$u = \mathrm{i}\{\epsilon u_1(x) + \epsilon^{\frac{3}{2}} u_2(x) + \ldots\} A(k,\omega)\, \mathrm{e}^{\mathrm{i}(ky-\omega t)}, \tag{3.1}$$

$$\bar{v} + v = \epsilon^{\frac{1}{2}} v_0(x) + \{\epsilon v_1(x) + \epsilon^{\frac{3}{2}} v_2(x) + \ldots\} A(k,\omega)\, \mathrm{e}^{\mathrm{i}(ky-\omega t)}, \tag{3.2}$$

$$\bar{h} + \eta = \epsilon^{\frac{1}{2}} h(x) + \{\epsilon \eta_1(x) + \epsilon^{\frac{3}{2}} \eta_2(x) + \ldots\} A(k,\omega)\, \mathrm{e}^{\mathrm{i}(ky-\omega t)}, \tag{3.3}$$

$$\omega = \omega_0 + \epsilon^{\frac{1}{2}} \omega_1 + \ldots, \tag{3.4}$$

where ϵ is a small perturbation parameter, $A(k,\omega)$ is the amplitude of the Kelvin wave, and ω and k are the wave frequency and the y-direction wavenumber, respectively.

Substituting the above expressions into (2.4)–(2.6) yields the first- and second-order linearized equation systems.

First order:

$$-\mathrm{i}\omega_0 u_1 - v_1 = -\eta_1', \tag{3.5}$$

$$-\mathrm{i}\omega_0 v_1 + u_1 = -\mathrm{i}k\eta_1, \tag{3.6}$$

$$-\mathrm{i}\omega_0 \eta_1 + u_1' + \mathrm{i}k v_1 = 0. \tag{3.7}$$

Second order:

$$-\mathrm{i}\omega_0 u_2 - v_2 = -\eta_2' - \mathrm{i}k v_0 u_1 + \mathrm{i}\omega_1 u_1, \tag{3.8}$$

$$-\mathrm{i}\omega_0 v_2 + u_2 = -\mathrm{i}k\eta_2 - \mathrm{i}k v_0 v_1 + \mathrm{i}\omega_1 v_1, \tag{3.9}$$

$$-\mathrm{i}\omega_0 \eta_2 + u_2' + \mathrm{i}k v_2 = -\mathrm{i}k v_0 \eta_1 - \mathrm{i}k h v_1 + \mathrm{i}\omega_1 \eta_1 - u_1 h' - u_1' h, \tag{3.10}$$

where a prime denotes the differential operator $\mathrm{d}/\mathrm{d}x$.

Both the first- and second-order solutions are subjected to the no-normal-velocity boundary condition at $x = 0$, and the solutions and their derivatives vanish when $x \to -\infty$, i.e.

$$u_1 = 0 \quad \text{at} \quad x = 0, \tag{3.11}$$

$$u_2 = 0 \quad \text{at} \quad x = 0, \tag{3.12}$$

$$(u_1, v_1, \eta_1), (u_1', v_1', \eta_1') \to 0 \quad \text{when} \quad x \to -\infty, \tag{3.13}$$

$$(u_2, v_2, \eta_2), (u_2', v_2', \eta_2') \to 0 \quad \text{when} \quad x \to -\infty. \tag{3.14}$$

The present perturbation analysis is valid only for long, low-frequency waves.

3.2. *Eigenvalue and eigenfunction solutions*

It is easy to verify that the first-order solution is the linear coastal Kelvin wave

$$u_1 = 0, \tag{3.15}$$

$$v_1 = \mathrm{e}^x, \tag{3.16}$$

$$\eta_1 = \mathrm{e}^x, \tag{3.17}$$

$$\omega_0 = k. \tag{3.18}$$

The actual amplitude of the Kelvin wave, $A(k,\omega)$, is already included in (3.1)–(3.3).

The second-order perturbation equations then can be derived as

$$u_2 = \frac{k[\eta_2' - \eta_2 + (c_{\mathrm{p}}^1 - v_0)\,\mathrm{e}^x]}{1-k^2}, \tag{3.19}$$

$$v_2 = \frac{\eta_2' - k^2[\eta_2 - (c_{\mathrm{p}}^1 - v_0)\,\mathrm{e}^x]}{1-k^2}, \tag{3.20}$$

$$\eta_2'' - \eta_2 = -2k^2(c_{\mathrm{p}}^1 - v_0)\,\mathrm{e}^x - (1-k^2)\,h\mathrm{e}^x + v_0'(x)\,\mathrm{e}^x - (1-k^2)\,h\,\mathrm{e}^x, \tag{3.21}$$

with the corresponding boundary conditions

$$\eta_2(0) - \eta_2'(0) - c_{\mathrm{p}}^1 + v_0(0) = 0, \tag{3.22}$$

$$\eta_2, \eta_2' \to 0 \quad \text{when} \quad x \to -\infty, \tag{3.23}$$

where $c_{\mathrm{p}}^1 = \omega^1/k$.

Through a change of variable, (3.21)–(3.23) become

$$Z_2'' - Z_2 = \phi(x), \tag{3.24}$$

$$Z_2(x) = Z_2'(x) \quad \text{when} \quad x = 0, \tag{3.25}$$

$$Z_2(x) = v_0(0) - c_p^1 \quad \text{when} \quad x \to -\infty, \tag{3.26}$$

$$Z_2'(x) = 0 \quad \text{when} \quad x \to -\infty, \tag{3.27}$$

where

$$Z_2 = \eta_2 + v_0(0) - c_p^1, \tag{3.28}$$

$$\phi(x) = -v_0(0) + c_p^1 - 2k^2(c_p^1 - v_0)\,e^x + v_0' e^x - (1-k^2)\,h\,e^x. \tag{3.29}$$

To satisfy the solvability condition so that $Z_2(x)$ has a non-trivial solution, $\phi(x)$ has to be orthogonal with the solution of the homogeneous equation, i.e.

$$\int_{-\infty}^{0} \phi(\xi)\,e^{\xi}\,d\xi = 0. \tag{3.30}$$

This yields the eigenvalue formula

$$c_p^1 = F(0), \tag{3.31}$$

where

$$F(x) = \int_{-\infty}^{x} [2v_0(\xi) + h(\xi)]\,e^{2\xi}\,d\xi. \tag{3.32}$$

Therefore, the effect of the horizontally sheared geostrophic mean current on the phase speed of the coastal Kelvin wave is a generalized Doppler shift, which is the weighted integration of the mean current velocity and the interface slope. Hence, the coastal Kelvin wave remains non-dispersive to the first order of the perturbation correction. A similar conclusion was reached by Grimshaw (1983) with a vertically sheared mean current.

The Green's function solution for Z_2 (see the Appendix) is

$$Z_2(x) = \int_{-\infty}^{0} \phi(\xi)\,G(x,\xi)\,d\xi, \tag{3.33}$$

where

$$G(x,\xi) = \begin{cases} \frac{1}{2}(e^{-x+\xi} - e^{x-\xi}) - \xi e^{x+\xi}, & x < \xi \leqslant 0 \\ \xi e^{x+\xi}, & -\infty < \xi < x. \end{cases} \tag{3.34}$$

Transforming Z_2 back to the original variable, η_2, and using (3.32) gives

$$\eta_2(x) = \frac{1-k^2}{2}\left\{e^{-x}F(x) + e^{x}\int_{x}^{0} [2v_0(\xi) + h(\xi)]\,d\xi\right\} - e^{x}[k^2 x F(0) + \tfrac{1}{2}v_0(0)]. \tag{3.35}$$

In this derivation, we have eliminated terms proportional to e^x, which are complementary solutions of (3.24). We also have eliminated any arbitrary constants created in the procedure of seeking perturbation solutions.

The eigenfunctions for $u_2(x)$ and $v_2(x)$ can be obtained by substituting the expression for $\eta_2(x)$ into (3.19) and (3.20):

$$u_2(x) = -k[e^{-x}F(x) - e^{x}F(0)], \tag{3.36}$$

$$v_2(x) = \eta_2(x) - e^{-x}F(x) + e^{x}v_0(x). \tag{3.37}$$

The above results show that in the presence of the mean current, the offshore velocity of a coastal Kelvin wave is no longer zero. However, it is still much smaller than the alongshore velocity, and its magnitude increases as the wave becomes shorter.

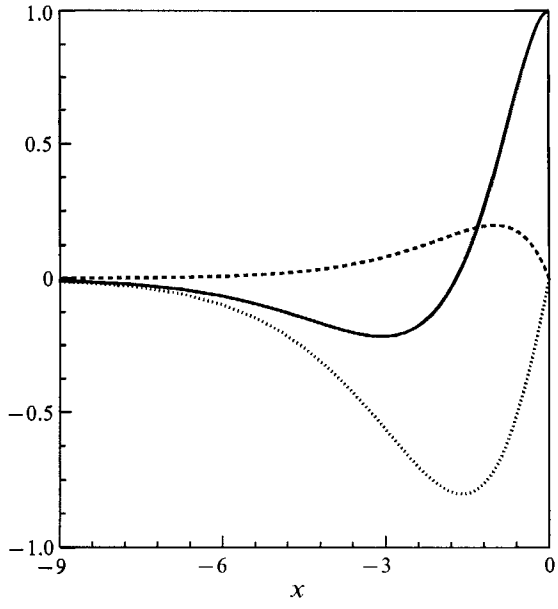

FIGURE 1. Zonal profiles of the second-order eigenfunctions, which are the corrections to the first-order coastal Kelvin wave due to a constant mean current $v_0 = -0.0185$. This non-dimensional current velocity is equivalent to a dimensional value of -0.05 m s^{-1} if the dimensional long-wave phase speed is assumed to be 2.7 m s^{-1}. Eigenfunctions are scaled such that $v_2(0) = 1$. The meridional wavenumber $k = 0.27$ and the eigenvalue phase speed $c_p = 0.98$. ----, u_2; ——, v_2; ·····, η_2.

In case of no zonal shear in the mean current, the solutions are simplified to

$$\eta_2(x) = \tfrac{1}{4}v_0 x\,\mathrm{e}^x[1-(1-k^2)x], \tag{3.38}$$

$$u_2(x) = -\tfrac{1}{2}v_0 k x\,\mathrm{e}^x, \tag{3.39}$$

$$v_2(x) = \tfrac{1}{4}v_0\,\mathrm{e}^x[1-x+(k^2-1)x^2], \tag{3.40}$$

$$c_p^1 = \tfrac{3}{4}v_0. \tag{3.41}$$

Again, we have eliminated the terms which are proportional to e^x in the expression for η_2.

Equation (3.41) is a little unexpected because the Doppler-shifted phase speed is $c+\frac{3}{4}v_0$ instead of $c+v_0$. Actually, the results are valid only for long Kelvin waves. As we will discuss later, the short Kelvin waves in a constant mean current, v_0, do have a Doppler-shifted phase speed of $c+v_0$.

Figure 1 displays the second-order eigenfunctions, which are the corrections to the Kelvin wave due to a constant mean current. They cause the Kelvin wave to be less confined to coastal areas. We checked the correctness of the analytical solution by directly solving the eigenvalue problem ((3.8)–(3.10), (3.12) and (3.14)) numerically. The solutions from these two methods agree so well that we cannot see any difference in the plots.

As the Kelvin wave becomes shorter, it will be more severely modified by second-order perturbation solutions until the maximum interface displacement no longer occurs at the eastern boundary, which is a feature of the so-called turning longitude problem. The perturbation scheme used in this section then breaks down because, for short waves, neglect of the wave–current interaction terms at the lowest level is no longer legitimate.

4. Short internal gravity waves trapped by geostrophic boundary current

We studied the effect on the internal Kelvin wave of a mean shear current which is assumed to have large alongshore scale ($\gg L_R$) and low frequency ($\ll f$), such that the linear theory is valid to the lowest order. However, as pointed out by Garrett & Munk (1975), measurements of low-frequency oceanic fluctuations are often obscured by high-frequency internal waves which are very energetic and have vertical and horizontal displacements of typically 10 m and 1 km. Pinkel (1983) observed that in the upper-ocean internal wave field off the coast of California the horizontal wavelength was $O(10\text{ km})$. Energetic small-scale waves in the upper pycnocline also were found by Webster (1968), and Kunze & Sanford (1984, 1986). Moreover, observations of the offshore structure and the alongshore-propagating pattern of the fluctuations in the eastern boundary currents suggest other interesting aspects which cannot be fully explained by the existing linear theory. According to Huyer (1990), the strongest fluctuations are not always found over the inner shelf, as is the situation over the Oregon shelf; sometimes the strongest fluctuations are over the midshelf, as occurs off both Peru and the southeastern Australian coasts. Even though the current fluctuation along the northwestern coast of the United States usually propagates northward, southward propagation is also observed. Huyer also pointed out that the coastal-trapped wave theory, which is basically linear, accounts reasonably well for large-scale, alongshore fluctuations, but it fails to explain the small-scale alongshore variations. These observations indicate that a nonlinear study of the trapped internal gravity waves in the boundary current is necessary. A first step in doing so is to include the wave–current interaction terms, which is the approach of the work in this section.

4.1. *Governing equations*

In addition to the assumptions made in §2, here we further assume that the mean current velocity is stronger than that caused by wave motion but weaker than the wave phase speed. As a result, the so-called critical layer (critical longitude in the present problem), where the mean current velocity equals the wave phase speed, will not be encountered.

We express the wave and mean current fields in the following form:

$$u = \mathrm{i}\epsilon U(x)\,\mathrm{e}^{\mathrm{i}(ky-\omega t)}, \tag{4.1}$$

$$\bar{v}+v = v_0(x)+\epsilon V(x)\,\mathrm{e}^{\mathrm{i}(ky-\omega t)}, \tag{4.2}$$

$$\bar{h}+\eta = h(x)+\epsilon Z(x)\,\mathrm{e}^{\mathrm{i}(ky-\omega t)}, \tag{4.3}$$

where the variables and parameters have the same meaning as before. In these perturbation expressions, the waves are assumed to be weaker than the mean current. Therefore, when the mean current diminishes, as will the wave field.

Then, (2.4)–(2.6) can be linearized as

$$[\omega-kv_0(x)]\,U-V = -Z', \tag{4.4}$$

$$-[\omega-kv_0(x)]\,V+[1+v_0'(x)]\,U = -kZ, \tag{4.5}$$

$$-[\omega-kv_0(x)]\,Z+[1+h(x)]\,U'+v_0(x)\,U+k[1+h(x)]\,V = 0, \tag{4.6}$$

where we have used the geostrophic relationships $v_0(x) = h'(x)$.

The boundary conditions to be imposed are

$$U = 0 \quad \text{at} \quad x = 0, \tag{4.7}$$

$$U, V, Z \to 0 \quad \text{as} \quad x \to -\infty. \tag{4.8}$$

Since the large-scale low-frequency waves are dominated by linear dynamics, we expect that, to the lowest order, the long waves in the present model are the internal Kelvin waves. This observation was confirmed by later numerical analysis in which we have found that all the long-wave eigenmodes are consistent with the analytical results given in §2.

In this section, we use the asymptotic method to study coastal-trapped internal gravity waves whose wavelengths are shorter than the internal Rossby radius of deformation. Since the phase speeds of these waves are close to 1 (the internal Kelvin wave speed), as shown later, this is equivalent to saying that the wave frequencies are higher than the inertial frequency. So, when we discuss short waves later, we also mean waves of high frequency.

The behaviour of short waves is dominated by the following equations:

$$U = -Z'/\{k[c_p - v_0(x)]\}, \tag{4.9}$$

$$V = Z/[c_p - v_0(x)], \tag{4.10}$$

$$Z'' - k^2\{1 - [c_p - v_0(x)]^2/[1 + h(x)]\}Z = 0, \tag{4.11}$$

with the boundary conditions in (4.7) and (4.8).

In deriving the above equations, we considered that the waves are of the quality of a boundary-layer phenomenon. The magnitude of Z' increases with k while that of Z does not (as shown in later asymptotic expressions for Z). We have neglected terms which are not important at large k. From the physical point of view, the simplification which led to (4.9)–(4.11) is consistent with the general belief that short waves have little to do with the Coriolis force. However, the Coriolis force in the present model affects the wave field indirectly through the lower-order current field, which is in geostrophic balance.

4.2. *A single-turning-longitude case*

The WKBJ solution for (4.11) is

$$Z \approx \frac{C_1 \cos\left[k\int^x (-q)^{\frac{1}{2}}\right]\mathrm{d}x + C_2 \sin\left[k\int^x (-q)^{\frac{1}{2}}\right]\mathrm{d}x}{(-q)^{\frac{1}{4}}} \quad (q < 0), \tag{4.12}$$

$$Z \approx \frac{C_3 \exp\left(k\int^x q^{\frac{1}{2}}\right)\mathrm{d}x + C_4 \exp\left(k\int^x -q^{\frac{1}{2}}\right)\mathrm{d}x}{q^{\frac{1}{4}}} \quad (q > 0), \tag{4.13}$$

where

$$q = 1 - [c_p - v_0(x)]^2/[1 + h(x)]. \tag{4.14}$$

Here, we assumed that q does not change sign in the vertical $(-\infty, 0]$, nor does it have zeros. Thus, there is no non-trivial solution which satisfies the evanescent condition at infinity if $q < 0$. The unique solution for $q > 0$ is

$$Z = \frac{C_4 \exp\left(-k\int^x q^{\frac{1}{2}}(x)\,\mathrm{d}x\right)}{q(x)^{\frac{1}{4}}}. \tag{4.15}$$

Hence, for large k

$$U = \frac{C_4 q^{\frac{1}{4}}(x)}{c_p - v_0(x)} \exp\left(-k\int^x q^{\frac{1}{2}}\mathrm{d}x\right). \tag{4.16}$$

Equations (4.7) and (4.16) lead to the dispersion relation

$$q(0) = 0. \tag{4.17}$$

This result contradicts our assumption that $q(x)$ does not vanish in the entire domain $(-\infty, 0]$. Therefore, the trapped *short* internal gravity waves in the mean current must have at least one turning longitude. In the following, we study trapped internal gravity waves with a single turning longitude.

4.2.1. *Eigenfunction solutions*

If (4.11) has the so-called turning longitudes, where q vanishes because of the existence of the geostrophic mean boundary current in the top layer, the WKBJ solution ceases to be valid nearby these points.

Assume that $x_0 < 0$ is a simple zero of $q(x)$, and that $x - x_0$ has the same sign as $q(x)$. Then, the eigenfunctions of (4.11) are

$$Z_1 \approx [q(x)/\zeta]^{-\frac{1}{4}} \operatorname{Ai}[k^{\frac{2}{3}}\zeta], \tag{4.18}$$

$$Z_2 \approx [q(x)/\zeta]^{-\frac{1}{4}} \operatorname{Bi}[k^{\frac{2}{3}}\zeta], \tag{4.19}$$

where

$$\left.\begin{aligned} \tfrac{2}{3}\zeta^{\frac{3}{2}} &= \int_{x_0}^{x} q^{\frac{1}{2}}(t)\,\mathrm{d}t \quad (x \geqslant x_0), \\ \tfrac{2}{3}(-\zeta)^{\frac{3}{2}} &= \int_{x}^{x_0} [-q(t)]^{\frac{1}{2}}\,\mathrm{d}t \quad (x \leqslant x_0). \end{aligned}\right\} \tag{4.20}$$

Ai, Bi are the first- and second-kind Airy functions (Olver 1974).

Because x_0 is a simple zero of $q(x)$, then $q'(x_0) \neq 0$. For large negative values of $k^{\frac{2}{3}}\zeta$

$$Z_1 \approx [-q(x)]^{-\frac{1}{4}} k^{-\frac{1}{6}} \sin[\tfrac{2}{3}k(-\zeta)^{\frac{3}{2}} + \tfrac{1}{4}\pi], \tag{4.21}$$

$$Z_2 \approx [-q(x)]^{-\frac{1}{4}} k^{-\frac{1}{6}} \cos[\tfrac{2}{3}k(-\zeta)^{\frac{3}{2}} + \tfrac{1}{4}\pi]. \tag{4.22}$$

Hence, Z_1 and Z_2 are identical to the WKBJ solution (4.12) when $x \to -\infty$ and $q(x) < 0$. They do not satisfy the vanishing boundary condition at infinity.

The only possibility for Z having a non-trivial solution is when $q(x)$ and $x - x_0$ have opposite signs. Then the expressions of the eigenfunctions of Z are identical to (4.18) and (4.19) but with the following definition of ζ:

$$\tfrac{2}{3}(-\zeta)^{\frac{3}{2}} = \int_{x_0}^{x} [-q(t)]^{\frac{1}{2}}\,\mathrm{d}t \quad (x \geqslant x_0), \tag{4.23}$$

$$\tfrac{2}{3}\zeta^{\frac{3}{2}} = \int_{x}^{x_0} q^{\frac{1}{2}}(t)\,\mathrm{d}t \quad (x \leqslant x_0). \tag{4.24}$$

From the behaviour of the Airy functions we know that when $x \to -\infty$

$$Z_1 \approx q^{-\frac{1}{4}}(x)\, k^{-\frac{1}{6}} \exp(-\tfrac{2}{3}k\zeta^{\frac{3}{2}}), \tag{4.25}$$

$$Z_2 \approx q^{-\frac{1}{4}}(x)\, k^{-\frac{1}{6}} \exp(\tfrac{2}{3}k\zeta^{\frac{3}{2}}). \tag{4.26}$$

Z_1 vanishes at infinity but Z_2 blows up when $x \to -\infty$. Thus, Z_2 should be eliminated from the eigenfunctions of the present problem. Z_1 exhibits oscillatory behaviour when $x > x_0$, and decays exponentially when $x < x_0$. In other words, Z_1 changes its behaviour through the turning longitude x_0 because of the characteristics of the Airy function $\operatorname{Ai}(y)$ on both sides of $y = 0$.

4.2.2. *Eigenvalue calculation*

We have shown that $q(x)$ must be of opposite sign to $x - x_0$ to have non-trivial solutions. Under this condition

$$Z \approx k^{-\frac{1}{6}}[-q(x)]^{-\frac{1}{4}} \sin[\tfrac{2}{3}k(-\zeta)^{\frac{3}{2}} + \tfrac{1}{4}\pi], \tag{4.27}$$

$$Z' \approx k^{\frac{5}{6}}[-q(x)]^{\frac{1}{4}} \cos[\tfrac{2}{3}k(-\zeta)^{\frac{3}{2}} + \tfrac{1}{4}\pi] + O(k^{-\frac{1}{6}}), \tag{4.28}$$

when $x \to 0$ and $k^{\frac{2}{3}}\zeta \to -\infty$.

Mode number (zonal)	Eigen-wavenumber	
	numerical method	asymptotic method
1	16.256	17.253
2	28.006	28.620
3	39.983	40.418
4	52.043	52.353
5	64.140	64.422
6	76.271	76.491
7	88.462	88.614
8	100.403	100.710
9	112.461	112.833
10	124.942	124.956

TABLE 1. Meridional (alongshore) wavenumbers of the ten lowest zonal modes with $c_p = 1.0$, which are trapped by a constant mean current $v_0 = -0.0185$. This non-dimensional current velocity is equivalent to a dimensional value of -0.05 m s^{-1}, if the dimensional long-wave phase speed is assumed to be 2.7 m s^{-1}. The eigenvalues (wavenumbers) are calculated numerically and by the asymptotic method.

Equations (4.7) and (4.9) and (4.28) yield the asymptotic equation for large k:

$$\cos\left[k\int_{x_0}^{0}(-q)^{\frac{1}{2}}\,\mathrm{d}x+\tfrac{1}{4}\pi\right]=0. \tag{4.29}$$

For a given value of the wavenumber, k, there are infinite number of c_p values satisfying (4.29). However, only a finite number of them belong to trapped waves because when c_p becomes too large, the turning longitude, x_0, even if it exists, will exceed the offshore range of a coastal-trapped phenomenon. Moreover, for a given boundary current with fixed width, there is a maximum value of $|c_p|$, beyond which waves cannot be trapped by the current.

If we use c_p as the eigenvalue, then (4.29) is extremely difficult to solve since q is a function not only of c_p, but also of the turning longitude, x_0. Instead, if we use k as the eignvalue for the given value of c_p, it greatly simplifies the problem. Since c_p is known, x_0 is determined and so is P, which is defined by

$$P=\int_{x_0}^{0}[-q(t)]^{\frac{1}{2}}\,\mathrm{d}t. \tag{4.30}$$

Now, the asymptotic dispersion relationship becomes

$$k=\frac{(4n+1)\,\pi}{4P}\quad(n=0,1,2,\ldots), \tag{4.31}$$

The above equation shows that for each given value of c_p we obtain an infinite number of eigenvalues k each of which corresponds to a distinct zonal mode. Also, for a fixed phase speed, or equivalently, for a fixed turning longitude, the alongshore wavenumber of a trapped internal gravity wave increases linearly with its zonal mode number. Equations (4.30)–(4.31) indicate that the amplitude of P is related to x_0; $k\to\infty$ if and only if $x_0\to 0$ (for any given n). Table 1 gives the eigenvalues of the ten lowest trapped zonal modes in a constant mean current. They were calculated both by the asymptotic method and by the numerical method that directly solves the linear eigenvalue system, (4.4)–(4.8).

In the limiting situation of x_0 approaching the eastern boundary $x = 0$, the dispersion relation (4.31) should be replaced by

$$c_p \to \pm 1 + v_0(0). \tag{4.32}$$

The sign of c_p should be opposite to that of $v_0'(0_-)$ due to the requirement $q'(0_-) < 0$, which is a necessary condition for the existence of trapped waves when $x_0 = 0$.

We call this group of trapped internal gravity waves, which have their turning longitude x_0 at the eastern boundary, the 'short Kelvin waves'. As shown in §4.4, the northward-propagating short Kelvin waves share the same dispersion curve as the classical Kelvin waves. These short Kelvin waves are nearly non-dispersive, and their Z-function also has an exponential offshore profile. The offshore decay ratio, however, is proportional to the alongshore wavenumber, k, and the wave is not in geostrophic balance at all. If the eastern boundary current varies a little within the internal Rossby radius of deformation, then the difference in phase speed between the Kelvin wave and the northward-propagating short Kelvin wave is about a quarter of the mean current speed (recall that the Doppler shifted phase speed of the Kelvin wave is $1 + \frac{3}{4}v_0$ for a constant mean current). If the mean current has a rapid zonal shear, then the phase speed of the short Kelvin wave is only affected by the velocity of the mean current at the eastern boundary.

4.3. *Current-shear-induced double-turning longitudes*

We have discussed the case of the single turning longitude in the last section, where the internal gravity wave guide is formed by the coastline and the turning longitude caused by the mean current. Now, we consider the situation in which the short internal gravity waves are trapped in a boundary current by two turning longitudes, which are some distance away from the coastline. We know that if the mean current velocity is zero, the only coastal trapped wave in the present model is the Kelvin wave; if the velocity of the geostrophic mean current does not vary in the offshort direction, then there can be, at most, one turning longitude. Therefore, if the geostrophic top-layer mean current induces more than one turning longitude for the internal gravity waves, it must have zonal shear.

4.3.1. *Eigenfunction solutions*

We assume that x_1 and x_2 are two simple turning longitudes, and $0 > x_1 > x_2$. To have non-trivial trapped modes, $q(x)$ must have the following characteristics:

$$\begin{aligned} q(x) > 0, \quad & x > x_1 \quad \text{or} \quad x < x_2, \\ q(x) < 0, \quad & x_2 < x < x_1, \\ q(x) = 0, \quad & x = x_1 \quad \text{or} \quad x = x_2. \end{aligned}$$

Let x^* be a point between x_1 and x_2, i.e. $x_2 < x^* < x_1$. Then, the solution for Z in each of the two regions $[x^*, 0]$ and $(-\infty, x^*]$ can be obtained by following the same procedure as for the single-turning-longitude case (Olver 1974):

$$Z_1 = [q(x)/\zeta_1(x)]^{-\frac{1}{4}}[c_1 \operatorname{Ai}(k^{\frac{2}{3}}\zeta_1) + c_2 \operatorname{Bi}(k^{\frac{2}{3}}\zeta_1)], \quad x^* \leqslant x \leqslant 0, \tag{4.33}$$

where

$$\zeta_1(x) = \begin{cases} \left\{\dfrac{3}{2}\displaystyle\int_{x_1}^{x} q^{\frac{1}{2}}(t)\,\mathrm{d}t\right\}^{\frac{2}{3}} & (x > x_1), \\ -\left\{\dfrac{3}{2}\displaystyle\int_{x}^{x_1} [-q(t)]^{\frac{1}{2}}\,\mathrm{d}t\right\}^{\frac{2}{3}} & (x < x_1); \end{cases} \tag{4.34}$$

and $$Z_2 = [q(x)/\zeta_2(x)]^{-\frac{1}{4}}[c_3 \operatorname{Ai}(k^{\frac{2}{3}}\zeta_2) + c_4 \operatorname{Bi}(k^{\frac{2}{3}}\zeta_2)], \quad -\infty < x \leqslant x^*, \tag{4.35}$$

where $$\zeta_2(x) = \begin{cases} -\left\{\frac{3}{2}\int_{x_2}^{x} [-q(t)]^{\frac{1}{2}}\,\mathrm{d}t\right\}^{\frac{2}{3}} & (x > x_2) \\ \left\{\frac{3}{2}\int_{x}^{x_2} q^{\frac{1}{2}}(t)\,\mathrm{d}t\right\}^{\frac{2}{3}} & (x < x_2). \end{cases} \tag{4.36}$$

To avoid the blowing up of $\operatorname{Bi}(k^{\frac{2}{3}}\zeta_1)$ at the coast for a large k, we have to make $c_2 = 0$; and because of the boundedness of Z at $-\infty$, c_4 also has to be zero.

4.3.2. *Eigenvalue calculation*

It remains to match the solutions of Z_1 and Z_2 at x^*.

The asymptotic expressions for Z_1 and Z_2 at x^* can be obtained according to the behaviour of Ai with large negative argument:

$$Z_1(x^*) \approx c_1 k^{-\frac{1}{6}}[-q(x^*)]^{-\frac{1}{4}} \sin\{\tfrac{2}{3}k[-\zeta_1(x^*)]^{\frac{3}{2}} + \tfrac{1}{4}\pi\}, \tag{4.37}$$

$$Z_2(x^*) \approx c_3 k^{-\frac{1}{6}}[-q(x^*)]^{-\frac{1}{4}} \sin\{\tfrac{2}{3}k[-\zeta_2(x^*)]^{\frac{3}{2}} + \tfrac{1}{4}\pi\}, \tag{4.38}$$

where $$[-\zeta_1(x^*)]^{\frac{3}{2}} = \frac{3}{2}\int_{x^*}^{x_1} [-q(t)]^{\frac{1}{2}}\,\mathrm{d}t, \tag{4.39}$$

$$[-\zeta_2(x^*)]^{\frac{3}{2}} = \frac{3}{2}\int_{x_2}^{x^*} [-q(t)]^{\frac{1}{2}}\,\mathrm{d}t. \tag{4.40}$$

A necessary condition for Z_1 and Z_2 to be matched at $x = x^*$ is that their Wronskian vanishes there (Jeffreys 1962; Olver 1974), i.e.

$$\begin{vmatrix} Z_1(x^*) & Z_2(x^*) \\ Z_1'(x^*) & Z_2'(x^*) \end{vmatrix} = 0. \tag{4.41}$$

For large k, the first derivatives of Z_1 and Z_2 can be approximated as

$$Z_1'(x^*) \approx -c_1 k^{\frac{5}{6}}[-q(x^*)]^{\frac{1}{4}} \cos\{\tfrac{2}{3}k[-\zeta_1(x^*)]^{\frac{3}{2}} + \tfrac{1}{4}\pi\}, \tag{4.42}$$

$$Z_2'(x^*) \approx c_3 k^{\frac{5}{6}}[-q(x^*)]^{\frac{1}{4}} \cos\{\tfrac{2}{3}k[-\zeta_2(x^*)]^{\frac{3}{2}} + \tfrac{1}{4}\pi\}. \tag{4.43}$$

Therefore, (4.41) leads to

$$\sin\{\tfrac{2}{3}k[-\zeta_1(x^*)]^{\frac{3}{2}} + \tfrac{2}{3}k[-\zeta_2(x^*)]^{\frac{3}{2}} - \tfrac{1}{2}\pi\} = 0, \tag{4.44}$$

which implies the dispersion relation

$$k = (2n+1)\pi/2P \quad (n = 0, 1, 2, \ldots), \tag{4.45}$$

where $$P = \int_{x^2}^{x_1} [-q(t)]^{\frac{1}{2}}\,\mathrm{d}t$$

(Olver 1974).

For high zonal modes, this dispersion relation is very close to that of the single (interior) turning longitude case. In fact, in the latter, the eastern boundary is acting as the other turning longitude. It is also true in the case of double turning longitudes, as for the single turning longitude, that the alongshore wavenumber of a trapped internal gravity wave increases with the zonal mode number, provided that the phase speed is fixed, or equivalently, the turning longitudes are fixed.

The boundary condition at $x = 0$, i.e. the normal velocity vanishes at the eastern boundary, is satisfied naturally to the first approximation because the solution, Z, has an evanescent characteristic for a large positive argument, $k^{\frac{2}{3}}\zeta(0)$.

4.3.3. *Wave guide location*

Owing to the zonal shear of the mean current, the internal gravity waves trapped in a wave guide formed by double turning longitudes behave differently from those which are trapped by a wave guide formed by the eastern boundary and a single interior turning longitude. In the former, the so-called shadow zones, where the internal gravity waves cannot propagate in the zonal direction but their amplitude decays exponentially, are on both sides of the wave guide. In the latter case, however, the shadow zone is only on the offshore side (western side) of the wave guide. The peak of a wave trapped in a double-turning-longitude wave guide is some distance away from the eastern boundary. It is desirable to know its location. Under the combined influences of current shear, interface slope, and the eastern boundary wall, these wave guides may occur in locations other than at the axes of the currents (Peregrine 1976) or the negative vorticity regions (Kunze 1985), as will be shown by the examples in §4.4.

The distance between turning longitudes, x_1 and x_2, is directly related to the phase speed, c_p. Thus, we can obtain their limit position, x^*, where x_1 and x_2 coincide, and the corresponding phase speed, c_p^*, by applying the Lagrangian-λ method for the variation of the function

$$\mathscr{F}(c_p, x) = c_p^2 \tag{4.46}$$

with two auxiliary conditions

$$1-[c_p-v_0(x)]^2/[1+h(x)] = 0, \tag{4.47}$$

$$\{1-[c_p-v_0(x)]^2/[1+h(x)]\}'' > 0. \tag{4.48}$$

The above problem can be modified as a variational problem about function $\hat{\mathscr{F}}$ by defining

$$\hat{\mathscr{F}}(c_p, x, \lambda) = c_p^2+\lambda\left[1-\frac{[c_p-v_0(x)]^2}{1+h(x)}\right], \tag{4.49}$$

where λ is an undetermined factor.

Now the values of x^*, c_p^* and λ of the free variation problem of $\hat{\mathscr{F}}$ can be found by

$$2c_p^*-2\lambda[c_p^*-v_0(x^*)]/[1+h(x^*)] = 0, \tag{4.50}$$

$$\lambda\left\{\frac{2[c_p^*-v_0(x^*)]\,v_0'(x^*)}{1+h(x^*)}+\frac{[c_p^*-v_0(x^*)]^2\,v_0(x^*)}{[1+h(x^*)]^2}\right\} = 0, \tag{4.51}$$

$$1-[c_p^*-v_0(x^*)]^2/[1+h(x^*)] = 0, \tag{4.52}$$

$$\{1-[c_p^*-v_0(x^*)]^2/[1+h(x^*)]\}'' > 0, \tag{4.53}$$

the solutions of which are

$$1-4[1+h(x^*)]\,v_0'^2(x^*)/v_0^2(x^*) = 0, \tag{4.54}$$

$$c_p^* = v_0(x^*)-2[1+h(x^*)]\,v_0'(x^*)/v_0(x^*), \tag{4.55}$$

$$\lambda = [1+h(x^*)]\,c_p^*/[c_p^*-v_0(x^*)], \tag{4.56}$$

together with condition (4.53) which is needed to identify false solutions.

This does not include the situation where x^* occurs on the eastern boundary; that issue was dealt with in §4.2.2.

4.4. *Three examples*

The interior current structure far away from the outmost longitude has virtually no effect on the internal gravity waves trapped in a wave guide that is close the eastern boundary; therefore, we only have to make the mean current structure of the model

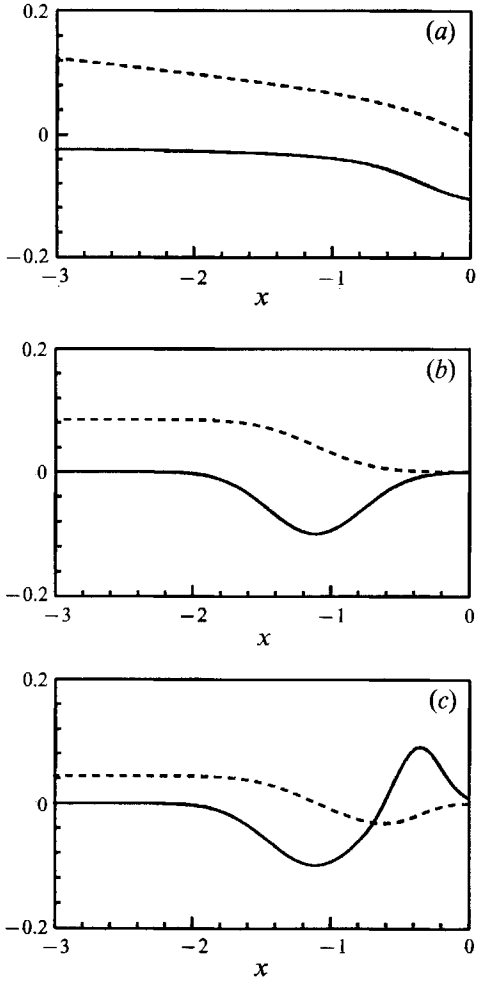

FIGURE 2. Zonal profiles of three examples of geostrophic mean currents and their corresponding upper-layer thickness displacements. Positive values of $h(x)$ mean that the layer is thicker than H_0, so that $h(x)$ contour is the mirror-image of the thermocline. (*a*) A broad southward current with its strong part at the eastern boundary; (*b*) a jet-like southward current; (*c*) a southward current with a countercurrent near the boundary. ----, $h(x)$; ——, $v_0(x)$.

resemble that of a real-world current within a distance that is wide enough to encompass the wave guide. Unless otherwise stated, the eigenvalue system, (4.4)–(4.8), is solved numerically. The results are then compared with the asymptotic results of the earlier sections.

The mean current (*a*) (figure 2*a*) is a broad, southward current that is strongest near the eastern boundary. It resembles the offshore profile of the California Current off Cape Mendocino (Hickey 1979).

Internal gravity waves trapped by this geostrophic mean current tend to have a single interior turning longitude if they are northward propagating (against the current); they have double interior turning longitudes if they are southward propagating (with the current). When the phase speed of the trapped internal gravity wave decreases, therefore, it is trapped by a narrower wave guide, the wave propagating against the mean current tends to be trapped close to the boundary, while the wave propagating with the mean current tends to be trapped toward x^*,

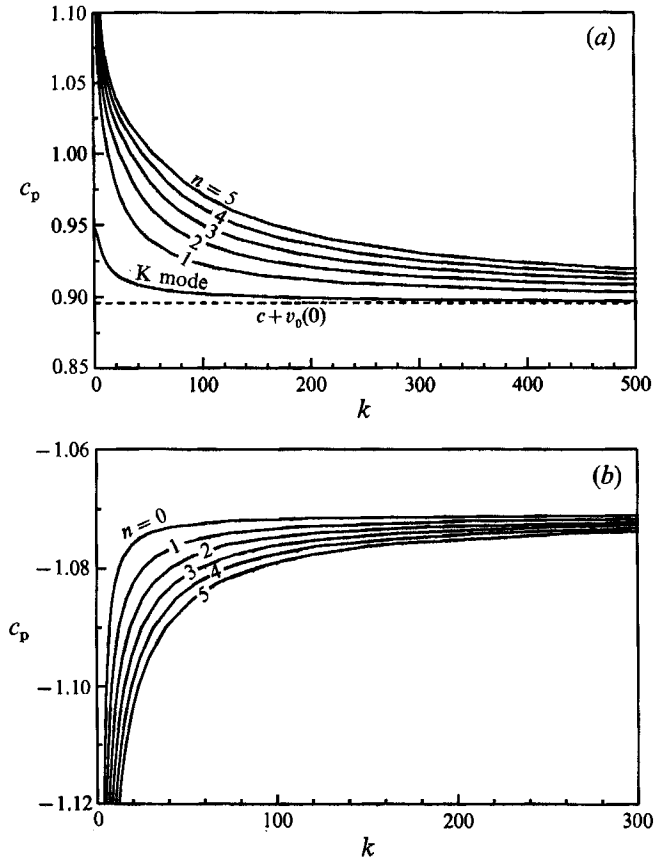

FIGURE 3. Dispersion relations of the six lowest trapped zonal modes of the internal gravity waves propagating against ($c_p > 0$), and following ($c_p < 0$), the southward mean current shown in figure 2(*a*).

Mean current type	Theoretical		Numerical	
	(x^*, c_p^*) $c_p^* > 0$	(x^*, c_p^*) $c_p^* < 0$	(x^*, c_p^*, k^*) $c_p^* > 0$	(x^*, c_p^*, k^*) $c_p^* < 0$
(*a*)	(0.000, 0.894)	(−1.222, −1.071)	(0.000, 0.894, 583.243)	(−1.225, −1.071, 317.495)
(*b*)	(−1.074, 0.919)	(0.000, −1.004)	(−1.061, 0.930, 44.761)	(0.000, −1.002, 139.271)
(*c*)	(−1.037, 0.899)	(−0.370, −0.899)	(−1.059, 0.910, 44.190)	(−0.363, −0.910, 92.792)

TABLE 2. Limit locations of the turning longitude, x^*, and the corresponding phase speeds, c_p^*. Results are calculated both the formulae given in §4.3.3 and by the numerical eigenvalue solver. k^* is the eigen-wavenumber obtained numerically.

which is the location of the wave guide formed by double interior turning longitudes in the short-wave limit. Good agreement is found between the numerical results and those predicted by the theories in §4.3.3 (table 2).

Figure 3 shows that when the wave phase speed increases, not only does the meridional (alongshore) wavenumber, k, of a given zonal mode becomes smaller but

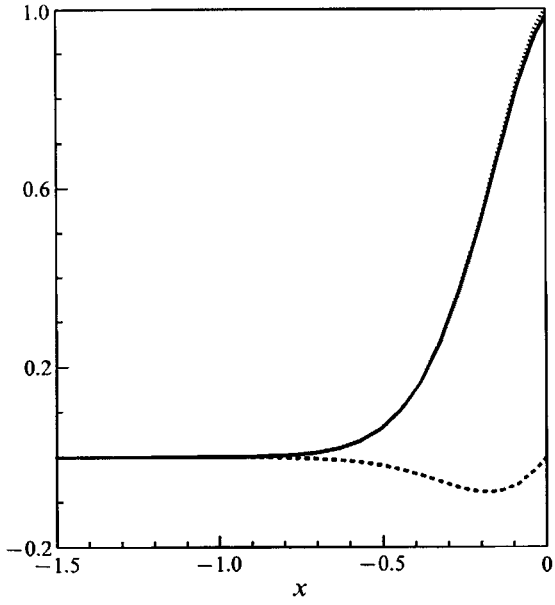

FIGURE 4. Offshore shape of a short Kelvin wave trapped by the mean current (*a*). $k = 27$ and $c_p = 0.912$. ----, u; ——, v; ·····, z. The curve z is so close to that of v that they can hardly be distinguished from each other in this figure.

the increment of k among different modes also decreases. For a given value of c_p, the increment of k is π/P (see (4.31) and (4.45)) each time the zonal mode number increases by 1. With a broad, southward, geostrophic mean current as current (*a*), π/P decreases rapidly with increasing c_p. Hence, the dispersion curves of different modes become focused at the long-wave end of the spectrum. The smallest alongshore wavenumber of the internal gravity waves trapped by current (*a*) is about 0.5, and the associated smallest increment of the wavenumber is about 0.3 between adjacent zonal modes. These values apply to both internal gravity waves with positive phase speed and to those with negative phase speed. This finding suggests that an energetic, internal gravity wave phenomenon, which is of wavelength comparable to the Rossby radius of deformation, or equivalently, of frequency comparable to the inertial frequency, may be formed simply because many more modes are trapped in the neighbourhood of this frequency than are trapped in the neighbourhoods of higher frequencies.

It is indicated by figure 3 that the long Kelvin waves in the boundary current are non-dispersive, which is consistent with the result of §3. Since the mean current (*a*) has negative vorticity at the coastline, northward-propagating short Kelvin waves are found. They are the continuation of the long Kelvin waves on the dispersion curve $n = 0$, $c_p > 0$. Their phase speed limit is $1+v(0)$, as stated by (4.32). Figure 4 displays the offshore shape of one of these short Kelvin waves. Its offshore decay ratio is much larger than that of classical Kelvin waves.

The eigenfunctions in figures 5 and 6 show that trapped internal gravity waves with the same phase speed have the same turning longitude. This is because c_p is the sole parameter which determines the zeros of $q(x)$.

In the present case, the eastern boundary acts as one of the turning longitudes for the northward-propagating, trapped internal gravity waves, both short and long (figure 5). However, the eastern boundary is not essential for trapping the southward-

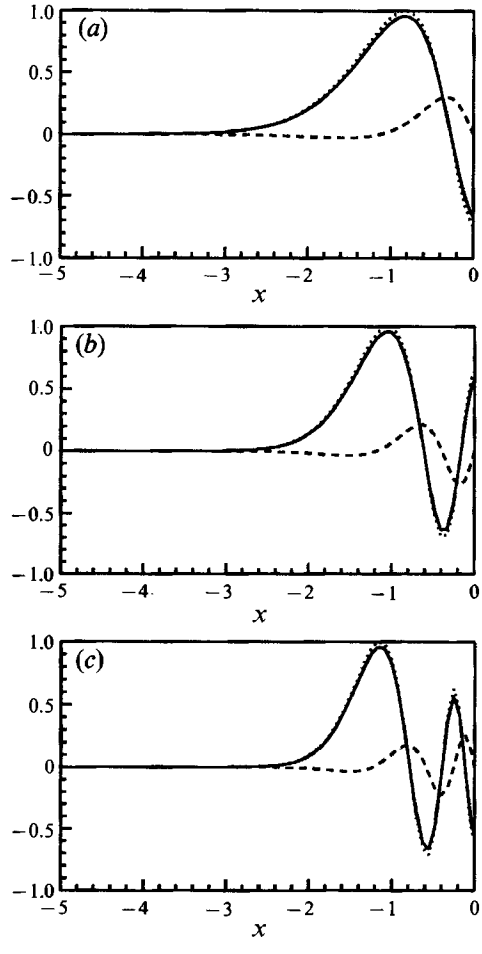

FIGURE 5. Offshore shapes of the three lowest zonal modes with $c_p = 1.01$. They are trapped by the mean current (*a*) and have a single turning longitude. (*a*) The $n = 1$ zonal mode with $k = 10.801$; (*b*) the $n = 2$ zonal mode with $k = 18.958$; (*c*) the $n = 3$ zonal mode with $k = 27.205$. – – –, u; ——, v; · · · · · ·, z. The curves of z are so close to those of v that they can hardly be distinguished from each other in this figure.

propagating waves (figure 6). Figure 7 tells us why this is so: the northward-propagating waves here can only have single interior turning longitudes, but the southward-propagating waves can have both single and double interior turning longitudes. The northward-propagating internal gravity waves here are trapped in a way similar to edge waves whose refraction is caused by offshore deepening in the absence of mean currents; in the case of double interior turning longitudes, however, the internal gravity wave energy is refracted away from the coast, against which the mean current is flowing.

The basic offshore features of the mean current (*b*) (figure 2*b*) resemble those of the California Current off Oregon, which was measured during the CUEI experiment (Hickey 1979). Compared with current (*a*), the new features introduced in this jet-like mean current (*b*) are that it has a positive vorticity zone on its eastern wing and that it is much narrower.

Because of a narrower boundary current, the turning longitudes of the internal

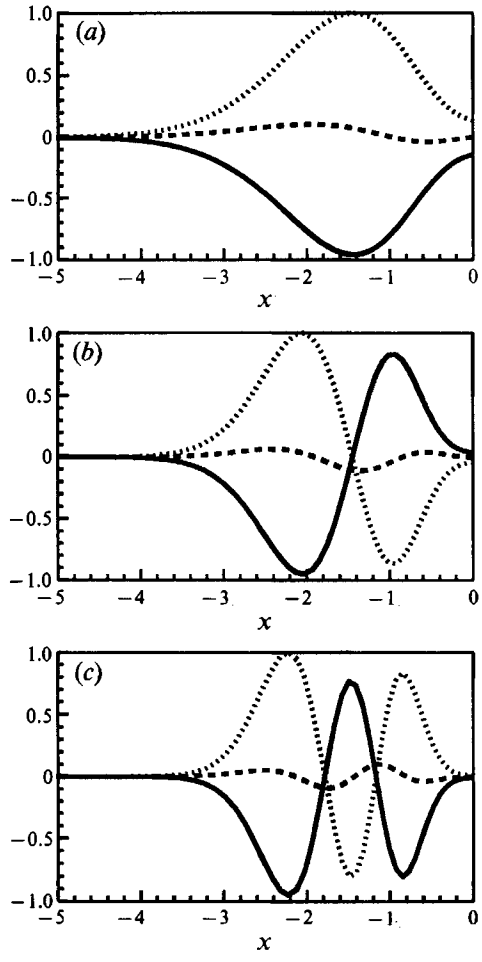

FIGURE 6. Offshore shapes of the three lowest zonal modes with $c_p = -1.08$. They are trapped by the mean current (*a*) and have double turning longitudes. (*a*) The $n = 0$ zonal mode with $k = 12.404$; (*b*) the $n = 1$ zonal mode with $k = 25.802$; (*c*) the $n = 2$ zonal mode with $k = 40.691$. – – –, u; ——, v; ·····, z.

gravity waves trapped by current (*b*) cannot go as far into the ocean's interior as those of the internal gravity waves trapped by current (*a*). A shorter distance between the turning longitudes (one of them may be the coastline) means a smaller phase speed of the internal gravity wave trapped in between them, which, in turn, means a larger longshore wavenumber (see (4.31) and (4.45)). Therefore, the maximum alongshore wavelength of the internal gravity waves (other than the Kelvin wave) trapped by current (*b*) is smaller than that of those trapped by current (*a*).

Figure 8 shows the interface displacements of two groups of fundamental modes in the offshore direction; one group propagates against the mean current ($c_p > 0$), the other with the mean current ($c_p < 0$). The ways that these modes are trapped by current (*b*), in terms of the number of interior turning longitudes, are opposite to those by current (*a*). Modes which propagate against current (*b*) tend to be trapped by double interior turning longitudes, while modes which propagate with current (*b*) tend to be trapped by a single interior turning longitudes. Since the axis of the jet

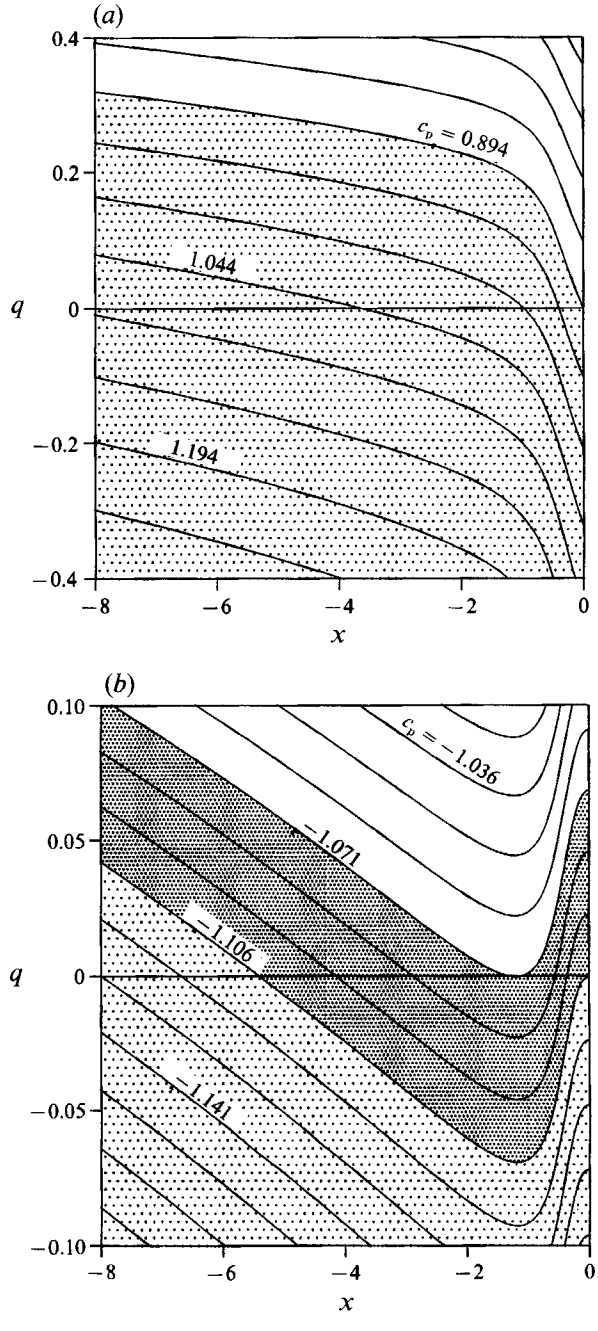

FIGURE 7. (*a*) $c_p(>0)$ isolines in the (x, q)-plane for the mean current type (*a*). The lightly shaded region covers c_p values which allow trapped gravity waves with a single turning longitude; c_p values in the unshaded region are too small for gravity waves to be trapped by the mean current. Isoline interval = 0.05. (*b*) Same as (*a*) but for $c_p < 0$. The darkly shaded region covers c_p values which allow trapped gravity waves with double turning longitudes. Isoline interval = 0.0117.

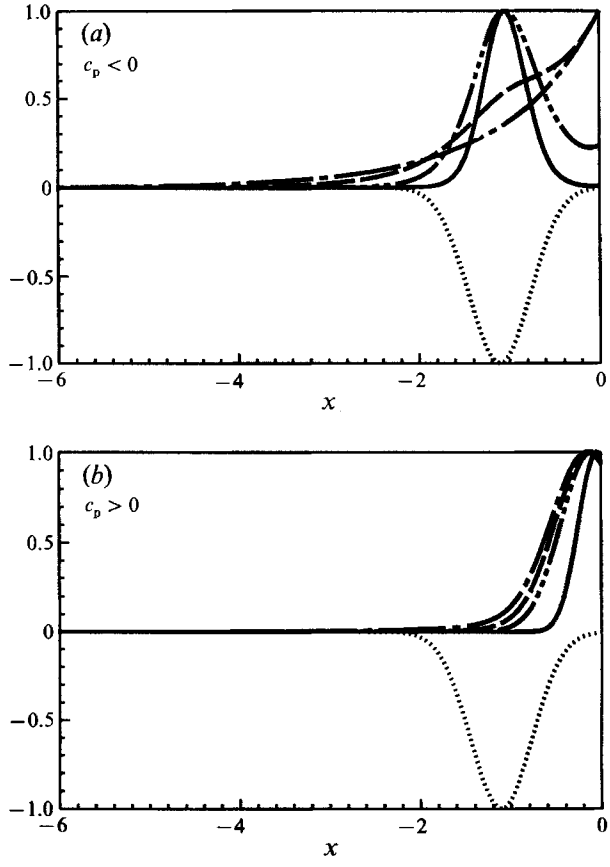

FIGURE 8. Interface displacement of eight fundamental zonal modes (four for $c_p > 0$ and four for $c_p < 0$), which are trapped by the mean current (*b*). (*a*) ——, $c_p = 0.94$, $k = 22.698$; ——·· ··——, $c_p = 0.96$, $k = 10.975$; – – –, $c_p = 0.98$, $k = 4.553$; ——·——, $c_p = 1.0$, $k = 1.445 \times 10^{-2}$; ·····, the mean current profile (with its actual magnitude multiplied by 10 (same in *b*)). (*b*) ——, $c_p = -1.01$, $k = 27.86$; ——·· ··——, $c_p = -1.02$, $k = 16.01$; – – –, $c_p = -1.03$, $k = 11.74$; ——·——, $c_p = -1.04$, $k = 9.531$.

is relatively far from the coastline, the internal Kelvin wave is hardly modified by the mean current (figure 8*a*).

Without boundaries and interface slope, a jet-like current cannot trap waves which propagate in the same direction (Peregrine 1976). Having included the boundary effect, current shear, and the interface (thermocline) slope, we find that this restriction is no longer true. The seaward deepening of the interface related to a southward geostrophic boundary current, small as it may be, can block southward-propagating internal gravity waves of certain parameter (c_p) range from transmitting into the western interior; they can be reflected back and forth between turning longitudes (one of them may be the eastern boundary) while they propagate with the mean current (figure 8*b*). Furthermore, the sign of the mean current vorticity is not a decisive factor in locating wave guides, as it was for the near-inertial waves in Kunze's (1985) study. Wave guides in the present study were formed in negative vorticity regions as well as in positive vorticity regions.

Figure 8 also indicates that as the phase speed becomes smaller, the northward-propagating waves are trapped closer to the limit position of the interior turning

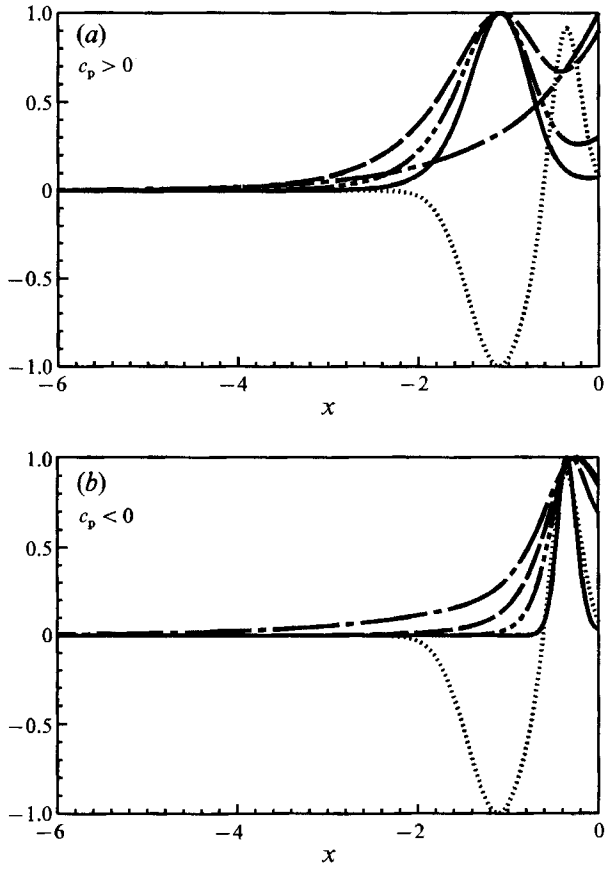

FIGURE 9. Interface displacement of eight fundamental eigenmodes (four for $c_p > 0$, four for $c_p < 0$) trapped by the mean current (c). (a) ——, $c_p = 0.96$, $k = 9.990$; ——···——, $c_p = 0.98$, $k = 7.036$; – – –, $c_p = 1.0$, $k = 4.895$; ——·——·, $c_p = 1.02$, $k = 9.396 \times 10^{-2}$; ·····, the mean current profile (with its actual magnitude multiplied by 10 (same in b)). (b) ——, $c_p = -0.92$, $k = 45.864$; ——···——, $c_p = -0.96$, $k = 12.336$; – – –, $c_p = -1.0$, $k = 6.822$; ——·——·, $c_p = -1.04$, $k = 4.862$.

longitude, x^*, which is coincident with the axis of current (b); meanwhile, the southward-propagating waves are trapped closer to the eastern boundary. The positive vorticity of mean current (b) at the coastline permits the southward-propagating short Kelvin waves, which are not allowed in current (a). They have the limiting phase speed of $-1+v_0(0)$.

The mean current in figure 2c has a countercurrent next to the boundary. In this case, the conditions $q(0) = 0$ and $q'(0) < 0$ cannot be satisfied simultaneously. As a result, the short Kelvin waves are not formed. Here, the internal gravity waves tend to be trapped by double turning longitudes, which have interior limit positions, x^* (table 2). Figure 9 shows that short internal gravity waves are trapped around one of the current axes, against which the waves are propagating.

The strong shear of the mean current (c) in the narrow northward-flowing region helps to trap southward-propagating internal gravity waves. Generally, however, if the northward geostrophic mean current is broad, the related interface slope, which shoals seaward, has the potential of leaking southward-propagating internal gravity waves into the western interior.

5. Conclusions and discussion

Using a reduced-gravity model, we found that geostrophic boundary currents not only modify the internal Kelvin wave, but also create wave guides which trap high-frequency, short internal gravity waves. These trapped internal gravity waves have phase speed close to that of the internal Kelvin wave, but the direction of their alongshore propagation can be the same as, or opposite to, that of the internal Kelvin wave. Their alongshore wavenumber increases with their offshore mode number, provided that the waves are trapped by the same wave guide.

The trapping mechanism of the internal gravity waves results from the combined effects of the current shear, the interface slope and the eastern boundary. However, wave guides that are much narrower than the Rossby radius of deformation are formed mainly because of the current shear, usually when the current is narrow or has a strong shear region. If the geostrophic mean current is wide, the associated interface slope plays an important role in forming wide wave guides. Since the maximum alongshore wavelength of the trapped internal gravity waves increases with the width of the wave guide, we expect that the spatial scale, and therefore the timescale, of the trapped internal gravity wave phenomenon caused by a wide geostrophic current will be larger than that due to a narrow current.

If there is no limit on the width of the geostrophic mean current, is it possible that the maximum alongshore wavelength of the trapped internal gravity wave can be indefinitely long? The answer is no. When the wavelength becomes longer, the role of the Coriolis force becomes more and more important, and the wave equations (4.9)–(4.11) become less and less accurate. Eventually, the primary balance switches to that between the pressure-gradient force and the Coriolis force. Then, the only trapped internal gravity wave left is the Kelvin wave. The alongshore wavenumbers of the longest waves (other than the Kelvin wave), which were found numerically in the examples of §4.4, are around 0.5. Thus, the Rossby radius of deformation and the inertial period are about the largest spatial and time scales that these trapped internal gravity waves can have. Interestingly, at this low-frequency end of the spectrum, the dispersion curves of different zonal modes become strongly focused, as shown in figure 3 with the example current (*a*). This suggests that an energetic internal gravity wave phenomenon with near-inertial frequency may be found in a broad geostrophic boundary current.

There are three constraints which lead to the trapped internal gravity waves having a small discrepancy in phase speed, assuming that they propagate in the same direction. Firstly, the boundary mean currents used in the present study are weak ($|v_0| \ll 1$) and have finite width. Therefore, the minimum value of $|c_p|$ of the internal gravity waves cannot be much less than the Kelvin wave speed in order for them to be trapped by the boundary current. If the phase speed is too small, turning longitudes cannot be created (see figure 7). For the prescribed mean current (*a*), the lower limit for $c_p > 0$ and upper limit for $c_p < 0$ as functions of k are guided by the two $n = 0$ dispersion curves in figure 3.

Secondly, there is a limitation on the maximum alongshore wavelength of the trapped internal gravity waves other than the Kelvin wave. This maximum wavelength is either comparable to the Rossby radius of deformation, or a function of the given boundary current, depending on which one is smaller. This, in turn, puts a restriction on the maximum value of $|c_p|$, since the maximum wave phase speed is associated with the maximum alongshore wavelength. Thus, if the width of mean current (*a*) is finite instead of being infinite, the offshore slope of the interface

vanishes beyond the longitudes where the mean current exists, then the magnitude of phase speed of trapped internal gravity waves has to be bounded, for turning longitudes can be created only within the width of the mean current. Therefore, the lower left corners of figure 7 (*a*, *b*), where large c_p isolines are, should be unshaded if the mean current (*a*) has a finite width.

Thirdly, the outermost turning longitude should be within a reasonable distance from the coastline for the trapped internal gravity waves to be considered as a coastal phenomenon. For a broad current, this means that $|c_p|$ should not greatly exceed 1. In fact, if we assume x_0 to be the outermost turning longitude, and $\bar{v}_0$ to be the average velocity of the boundary current $v_0(x)$ within $[x_0, 0)$, then

$$c_p = \pm(1+\bar{v}_0 x_0)^{\frac{1}{2}} + v_0(x_0). \tag{5.57}$$

According to this estimation, $|c_p|$ is only about 1.14 if $x_0 = -30$ and $\bar{v}_0 = -0.01$. Therefore, for realistic basin size and parameters which describe the mean boundary current, the range of c_p is confined within two narrow regions near $c_p = 1$ and $c_p = -1$, rather than being limitless.

In order for the shallow-water equation to be valid, k (non-dimensional) should be smaller than $g'^{\frac{1}{2}}/(2fH_0^{\frac{1}{2}})$. Therefore, k is allowed to have larger values in lower latitudes, where L_R is larger, than in higher latitudes, assuming that H_0 and g' are unchanged. Given $g' = 0.04\ \mathrm{m\ s^{-2}}$ and $H_0 = 40$ m, k_{max} is around 200 for a mid-latitude ocean. So, the large k values in figure 3 would require a shallower or stronger thermocline, or a lower latitude ocean.

Most of this work is based on the Part II of the author's Ph.D. dissertation. Many thanks are due to her thesis advisor, Professor John P. Boyd, for his continued discussion and help. The author is also grateful to Professor Stanley J. Jacobs for pointing out a mistake in an earlier draft of the thesis; and to Professor Guy A. Meadows for many helpful discussions. The author is indebted to two anonymous referees, whose comments helped to improve the quality of this paper. This work received support from The National Science Foundation through grants OCE8509923, OCE8812300, DMS8716766; and from The Department of Atmospheric, Oceanic and Space Sciences of The University of Michigan.

Appendix. Derivation of the Green's function for Z_2

If (3.24) is multiplied by G and then integrated from minus infinity to zero, we obtain

$$\int_{-\infty}^{0} [Z_2''(\xi) - Z_2(\xi)]\, G(x,\xi)\, \mathrm{d}\xi = \int_{-\infty}^{0} \phi(\xi)\, G(x,\xi)\, \mathrm{d}\xi. \tag{A 1}$$

Applying the partial integration rule to the left-hand side of (A 1) yields

$$Z_2'(0)\, G(x,0) - Z_2'(-\infty)\, G(x,-\infty) - [Z_2(0)\, G_\xi(x,0) - Z_2(-\infty)\, G_\xi(x,-\infty)] + \int_{-\infty}^{0} Z_2(\xi)\, [G_{\xi\xi}(x,\xi) - G(x,\xi)]\, \mathrm{d}\xi. \tag{A 2}$$

Imposing the boundary conditions of Z_2 and requiring that $G_\xi(x,-\infty) = 0$ yields

$$Z_2'(0)\, [G(x,0) - G_\xi(0)] + \int_{-\infty}^{0} Z_2(\xi)\, [G_{\xi\xi}(x,\xi) - G(x,\xi)] = \int_{-\infty}^{0} \phi(\xi)\, G(x,\xi)\, \mathrm{d}\xi. \tag{A 3}$$

Now the Green's function $G(x,\xi)$ is determined by

$$G_{\xi\xi}-G=\delta(x-\xi)+F, \tag{A 4}$$

$$G(x,0)-G_{\xi}(x,0)=0, \tag{A 5}$$

$$G_{\xi}(x,-\infty)=0, \tag{A 6}$$

where $F=-2\,\mathrm{e}^{x+\xi}$. The reason for the existence of F is to make the right-hand side of (A 4) orthogonal to the function e^{ξ}, which is a complementary solution (Greenberg 1971).

From (A 4) we derive

$$G(x,\xi)=\begin{cases}A\,\mathrm{e}^{\xi}+B\,\mathrm{e}^{-\xi}-\xi\,\mathrm{e}^{x+\xi}, & x<\xi\leqslant 0\\ D\,\mathrm{e}^{\xi}+E\,\mathrm{e}^{-\xi}-\xi\,\mathrm{e}^{x+\xi}, & -\infty<\xi<x\end{cases} \tag{A 7}$$

where A, B, C and D are constants to be determined.

In order to satisfy the vanishing boundary condition (A 6), E must be zero. Furthermore, the continuity condition of G at $\xi=x$ leads to

$$A\,\mathrm{e}^{x}+B\,\mathrm{e}^{-x}=D\,\mathrm{e}^{x}. \tag{A 8}$$

Equations (A 5) and (A 7) yield

$$B=-\tfrac{1}{2}\mathrm{e}^{x}. \tag{A 9}$$

By integrating (A 4) with ξ once in the interval $[x-0,x+0]$ we obtain

$$G_{\xi}|_{x-0}^{x+0}-\int_{x-0}^{x+0}G\,\mathrm{d}\xi=1+\int_{x-0}^{x+0}F\,\mathrm{d}\xi. \tag{A 10}$$

Taking into consideration the continuity requirement of functions G and F at $\xi=x$, the above equation gives

$$G_{\xi}|_{x-0}^{x+0}=1. \tag{A 11}$$

Substituting the expression for $G(x,\xi)$ given in (A 7) into (A 11) gives

$$A\,\mathrm{e}^{x}-B\,\mathrm{e}^{-x}-D\,\mathrm{e}^{x}=1. \tag{A 12}$$

Equations (A 8), (A 9) and (A 12) yield

$$A=\tfrac{1}{2}\mathrm{e}^{-x}+D, \tag{A 13}$$

$$D=D(x), \tag{A 14}$$

where $D(x)$ is an arbitrary function of x because e^{ξ} is a complementary solution.

From (A 3)–(A 6) we obtain

$$Z_2(x)=-\int Z_2F\,\mathrm{d}\xi+\int_{-\infty}^{0}\phi(\xi)\,G(x,\xi)\,\mathrm{d}\xi=K_1\,\mathrm{e}^{x}+\int_{-\infty}^{0}\phi(\xi)\,G(x,\xi)\,\mathrm{d}\xi, \tag{A 15}$$

where $K_1=2\int_{-\infty}^{0}Z_2(\xi)\,\mathrm{e}^{\xi}\,\mathrm{d}\xi$ is an arbitrary constant.

REFERENCES

Boyd, J. P. 1989 *Chebyshev and Fourier Spectral Methods*. Springer.

Garrett, C. & Munk, W. 1975 Space-time scales of internal waves: a progress report. *J. Geophys. Res.* **80**, 291–297.

Greenberg, M. D. 1971 *Applications of Green's Function in Science and Engineering*. Prentice-Hall.

GRIMSHAW, R. 1983 The effect of a mean current on Kelvin waves. *J. Phys. Oceanogr.* **13**, 43–53.

GRIMSHAW, R. & YI, Z.-X. 1990 Finite amplitude long waves on coastal currents. *J. Phys. Oceanogr.* **20**, 3–20.

HICKEY, B. M. 1979 The California current system – hypotheses and facts. *Prog. Oceanogr.* **8**, 191–279.

HUYER, A. B. 1990 Shelf circulation. *The Sea* **9**, 423–493.

JEFFREYS, H. 1962 *Asymptotic Approximations*. Oxford University Press.

JOHNSON, J. W. 1947 The refraction of surface waves by currents. *Trans. Am. Geophys. Union* **28**, 867–874.

JONSSON, I. G. 1989 Wave-current interactions. *The Sea* **9**, 65–120.

KENYON, K. E. 1971 Wave refraction in ocean currents. *Deep-Sea Res.* **18**, 1023–1034.

KUNZE, E. 1985 Near-inertial wave propagation in geostrophic shear. *J. Phys. Oceanogr.* **15**, 544–565.

KUNZE, E. & SANFORD, T. B. 1984 Observations of near-inertial waves in a front. *J. Phys. Oceanogr.* **14**, 566–581.

KUNZE, E. & SANFORD, T. B. 1986 Near-inertial wave interactions with mean flow and bottom topography near Caryn Seamount. *J. Phys. Oceanogr.* **16**, 109–120.

LONGUET-HIGGINS, M. S. & STEWART, R. W. 1960 Changes in the form of short gravity waves on long waves and tidal currents. *J. Fluid Mech.* **8**, 565–583.

LONGUET-HIGGINS, M. S. & STEWART, R. W. 1961 The Changes in the amplitude of short gravity waves on steady non-uniform currents. *J. Fluid Mech.* **10**, 529–549.

MA, H. 1991 Studying nonlinear equatorial dynamics with a spectral element shallow water equation model and internal gravity wave guide in boundary current. Ph.D. thesis. The University of Michigan.

OLVER, F. W. J. 1974 *Asymptotics and Special Functions*. Academic.

PEREGRINE, D. H. 1976 Interaction of water waves and currents. *Adv. Appl. Mech.* **16**, 9–117.

PEREGRINE, D. H. & SMITH, R. 1975 Stationary gravity waves on non-uniform free streams: jet-like flows. *Math. Proc. Camb. Phil. Soc.* **77**, 415–438.

PINKEL, R. 1983 Dopplar sonar observations of internal waves: wavefield structure. *J. Phys. Oceanogr.* **13**, 804–815.

SMITH, R. 1970 Asymptotic solutions for high frequency trapped wave propagation. *Phil. Trans. R. Soc. Lond.* A **268**, 289–324.

UNNA, P. J. H. 1942 Waves and tidal streams. *Nature* **149**, 219–220.

WEBSTER, F. 1968 Observations of the inertial period motions in the deep sea. *Rev. Geophys.* **6**, 473–490.